ROYAL SOCIETY
OF CHEMISTRY

## PAPER

Check for updates

# Acid–base concentration swing for direct air capture of carbon dioxide†

Anatoly Rinberg (iD) * and Michael J. Aziz (iD)

This work demonstrates the first experimental evidence of the acid–base concentration swing (ABCS) for direct air capture of $CO_2$. This process is based on the effect that concentrating particular acid–base chemical reactants will strongly acidify solution, through Le Chatelier's principle, and result in outgassing absorbed $CO_2$. After collecting the outgassed $CO_2$, diluting the solution will result in a reversal of the acid–base reaction, basifying the solution and allowing for atmospheric $CO_2$ absorption. The experimental study examines a system that includes sodium cation as the alkalinity carrier, boric acid, and a polyol complexing agent that reversibly reacts with boric acid to strongly acidify solution upon concentration. Though the tested experimental system faces absorption rate and water capacity limitations, the ABCS process described here provides a basis for further process optimization. A generalized theoretical ABCS reaction framework is developed and different reaction orders and conditions are studied mathematically. Higher order reactions yield favorable cycle output results, reaching volumetric cycle capacity above 50 mM for third-order and 80 mM for fourth-order reactions. Optimal equilibrium constants are determined in order to guide alternative chemical searches and synthetic chemistry design targets. There is a substantial energetic benefit for reaction orders above the first, with second- and third-order ABCS cycles exhibiting a thermodynamic minimum work for the concentrating and outgassing steps around 150 kJ per mole of $CO_2$. A significant advantage of the ABCS is that it can be driven through well-developed and widely-deployed desalination technologies, such as reverse osmosis, with opportunities for energy recovery when recombining the concentrated and diluted streams, and extraction can occur directly from the liquid phase upon vacuum application.

## 1 Introduction

Carbon dioxide removal has emerged as a key component of addressing global climate change, necessary for compensating for hard-to-avoid emissions from industries such as agriculture and aviation.[1,2] With global warming exceeding 1.3 °C,[3] and already harming the most vulnerable and underprivileged populations on this planet, carbon removal will likely need to reach a scale of gigatonnes of $CO_2$ per year. However, the international scientific community is in agreement that reducing greenhouse gas emissions must be prioritized to avert the worst harms of climate change.[4] Some have called for decoupling emission reduction and carbon dioxide removal targets, to avoid the dangers of mitigation deterrence and the associated moral hazard, which follow from setting massive carbon dioxide removal targets of 10–20 $GtCO_2$ per year.[5]

*John A. Paulson School of Engineering and Applied Sciences Harvard University Cambridge, Massachusetts, 02138, USA. E-mail: rinberg@g.harvard.edu*

### 1.1 Direct air capture

Carbon dioxide removal spans a broad range of approaches, from land and ocean-based methods, such as reforestation, shifts in agricultural practices, and the addition of alkalinity into the ocean, to industrial methods, such as enhanced mineralization and direct air capture with carbon storage (DACCS).[6,7] DACCS, in particular, is a highly energy-intensive chemical process for capturing atmospheric $CO_2$, concentrating and compressing it, and then durably storing it in geological reservoirs or materials. Although exceptions exist, DAC methods are broadly split into two categories: one that is based on a solid sorbent and another that relies on solvent contacting. Each approach confers its own advantages. Solid sorbents, which often rely on amine polymers to react with $CO_2$, require only low-grade heat or moisture for regeneration, and rely on minimal water usage.[8] Solvent-based approaches, on the other hand, require large amounts of water, but have the advantage of decoupling contacting from regeneration allowing for continuous absorption.[9]

In particular, electrochemical aqueous solvent DAC approaches are being investigated extensively.[10–14] One type of

electrochemical DAC can be driven by changing the charge state of a redox-active molecule to either directly bind with dissolved inorganic carbon (DIC) or indirectly control the hydroxide concentration in solution. Such systems have the advantage of feasibly reaching low energy of capture, below 100 kJ mol$^{-1}$; however, the proposed approaches face a range of implementation challenges, such as chemical degradation, membrane stability and fouling, low kinetics of reaction.[15] Other electrochemical approaches are driven through electrolysis reactions to create a stream of base and acid, for $CO_2$ capture and subsequent neutralization, respectively.[16]

In contrast, the approach explored in this work, the acid–base concentration swing (ABCS), is based on a new driving method that controls the concentration of solutes in solution. No redox reaction is involved, nor is the addition or removal of acids or bases from solution. Osmotic pressure drive, such as through reverse osmosis, can be used to control the concentration of reactants in solution. In this way, though finding reversible and stable candidate reactions, as well reaching high absorption kinetics, pose challenges, the ABCS paradigm opens the exploration of new aqueous DAC chemistry.

### 1.2 Enhancing the alkalinity concentration swing with acid–base reactions

Our previous work, characterizing the alkalinity concentration swing (ACS), reported a process driven by concentrating an alkaline solution loaded with DIC captured from atmospheric $CO_2$. Increasing the alkalinity and DIC concentrations together increases the solution partial pressure of $CO_2$ and allows for $CO_2$ collection upon vacuum application. However, the ACS, without modification, requires excessive amounts of water and has an extremely slow characteristic absorption timescale due to the requirement that it operate close to equilibrium with atmospheric $CO_2$.

We have since improved on the ACS process, by proposing the addition of a step that selects between bicarbonate and carbonate ions, which increases the volumetric cycle capacity and the absorption rate.[17–19] In this work, we propose yet another modification to the ACS, the acid–base concentration swing, which introduces additional acid and base molecules into the solvent to enhance the cycle output. The relation between the alkalinity carrier, the DIC system, and the acid–base system through reaction with water, protons, and hydroxides allows for a wide range of solution state control that can be driven through osmotic pressure. The fundamental concept underlying the ABCS enhancement is the concentration-dependent charge competition between DIC anions and the added acid anions in solution. The non-conservative nature of DIC species and the ability for carbon species to be uncharged in the form of aqueous $CO_2$ allows for shifting the equilibrium between DIC species in a favorable way as the solution is concentrated and diluted. At dilute concentrations the added acid is un-dissociated, and thereby uncharged, and the DIC anions, bicarbonate and carbonate, dominate. As the solution is concentrated, the acid anions replace bicarbonate and carbonate ions as negative charge carriers, shifting the DIC species

to aqueous $CO_2$, which therefore increases the solution partial pressure of $CO_2$.

### 1.3 Non-linear chemical reactions

To develop a theoretical framework for the ABCS, we relied on past literature of non-linear chemical reactions.[20,21] The ABCS efficiency increases as cooperativity and non-linearity of the underlying chemical reactions increase. Other chemical systems, such as pH oscillators,[22–24] which can persist in isolated systems driven solely through chemical potential, and which exhibit complicated spatial and temporal behaviors, have been studied extensively and also rely on non-linear, cooperative reactions. The existence and wide-range of such non-linear chemical interactions suggests the potential of identifying and engineering chemical systems optimal to the ABCS.

Most famously, Belousov–Zhabotisnky reactions have been studied as a model chemical oscillator based on bromine chemistry;[25] however its reaction occurs at highly acidic conditions, making it inapplicable to high pH capture. The boric acid and polyol system, which we discuss later in this work, is better matched to the ABCS due to higher p$K_a$ values, and it exhibits the desired qualitative behavior required for the ABCS.[26] Polyols, such as Mannitol or Sorbitol, react with boric acid reversibly to increase its acidity, or lower its effective p$K_a$. Concentrating these molecules together will, therefore, strongly decrease the pH of the solution and enhance $CO_2$ outgassing. Though the equilibrium constants of the boric acid and polyol system are not in the optimal range for the ABCS, the system serves as a first existence proof for non-linear acid–base systems that can be further developed or synthetically designed.
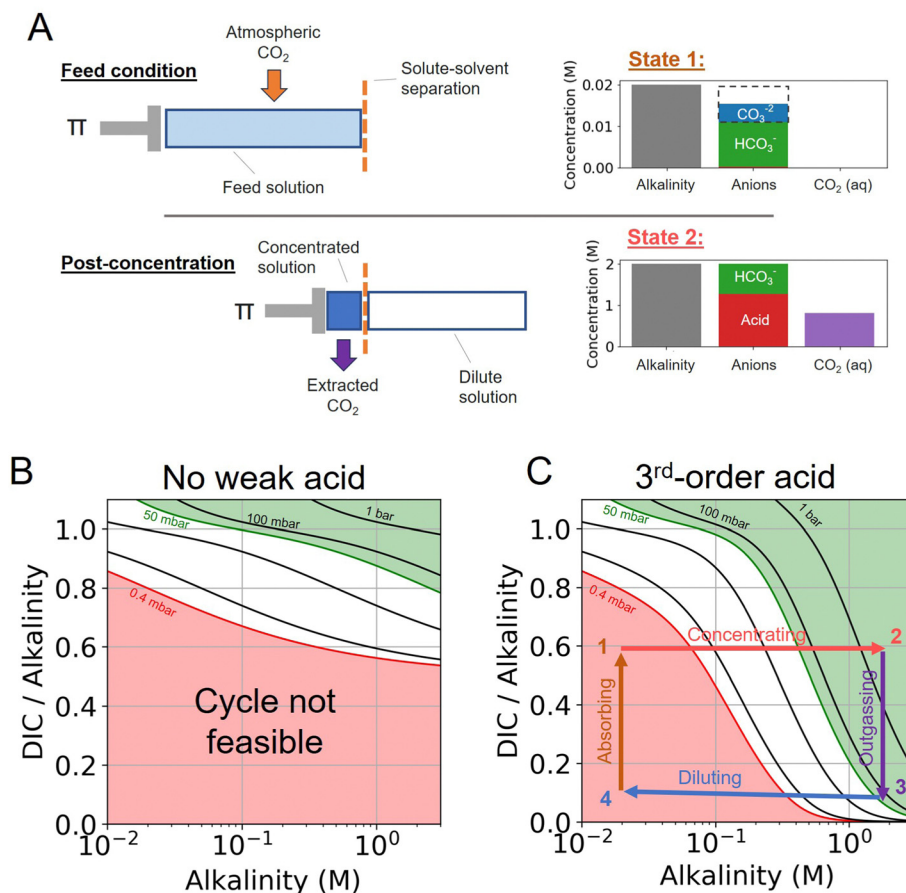
## 2 Acid–base concentration swing (ABCS): process description

The $CO_2$ separation processes explored in this work is based on the principle that the concentration and dilution of an alkaline solution shifts the solution partial pressure of $CO_2$. Here, we expand on principle of the previously reported alkalinity concentration swing,[27] and evaluate the addition of various weak acid and complexing agents to enhance the concentration swing mechanism.

Different acid–base reaction orders will exhibit different pH scaling properties, based on Le Chatelier's Principle, as solutes are concentrated or diluted. This pH control can be combined with an alkaline aqueous system to drive $CO_2$ absorption and outgassing. We find that the addition of higher-order acid–base reactions could be used to enhance the outgassing of $CO_2$ by rapidly decreasing the pH of the solution as the ions in solution are concentrated. To evaluate the system analytically, we separate the system into three components (Fig. 1).

First, the alkalinity carrier: the alkalinity carriers in our system are equivalent to strong base cations (denoted by $[B^+]$ in this work), such as sodium or potassium. The alkalinity provides a positive charge in solution, but does not directly interact with any other component of the system.

Fig. 1   Acid–base concentration swing schematic. (A) Top panel: The feed condition at 20 mM is depicted corresponding to State 1 in (C). At dilute concentrations, no weak acid anions are present and solution partial pressure of $CO_2$ is low. The dashed box represents the charge concentration of carbonates (at $-2$ charge per ion) to illustrate that charge neutrality is maintained. Bottom panel: The post-concentration solution at 2 M is depicted corresponding to State 2 in (C). $\Pi$ represents the osmotic pressure necessary for solvent–solute separation. The weak acid is the dominant anionic species, which results in non-charged DIC to be present in the form of aqueous $CO_2$. (B) A DIC-to-alkalinity schematic depicted modeled solution states with only alkalinity and DIC present. (C) A DIC-to-alkalinity schematic depicting a modeled 3rd-order acid system with an overlayed ABCS cycle.

Second, the acid–base system: the addition of a weak acid and/or bases, as well as non-charged complexing agents (denoted by L), can be added to solution to add proton and hydroxide sinks and sources for the DIC species to exchange with. For simplicity, we only consider acid–base species that mediate interactions through the aqueous solvent, and do not interact directly with DIC species (*e.g.* such as binding of $CO_2$ and amines to form carbamates).

Third, dissolved inorganic carbon (DIC): aqueous $CO_2$, bicarbonate, and carbonate concentration and speciation are determined for different conditions, either at fixed DIC or fixed $CO_2$ partial pressure.

When no additional acid–base species are introduced, the system is equivalent to the alkalinity concentration swing process (Fig. 1B). There is no feasible DAC cycle possible under these conditions.

The interactions between the three components above are subject to the following two conditions: (1) charge neutrality and (2) reactions between systems are mediated through $H^+$ and $OH^-$ or, in other words, protons and hydroxide ions are the only species exchanged between the DIC and acid–base systems.

The states of the ABCS cycle are best represented by the arrows overlaid on the DIC-to-alkalinity diagram in Fig. 1C. This is because in a plot of DIC-to-alkalinity *vs.* alkalinity, concentrating and diluting steps are represented simply by horizontal lines. The ABCS cycle is described succinctly as follows:

• Step 1 → 2: concentrating acids and bases – alkalinity, DIC, and acid–base system are concentrated together. Alkalinity is used as a reference concentration, and all other species concentrations are defined in relation to alkalinity.

• Step 2 → 3: $CO_2$ outgassing – vacuum is applied and the solution $CO_2$ partial pressure is taken to $p_{out}$, thereby outgassing and collecting $CO_2$. The collected $CO_2$ quantity, or the volumetric cycle capacity, $C_{out}$, is defined in terms of moles of $CO_2$ collected per volume of feed solution.

• Step 3 → 4: diluting acids and bases – the concentrated solution, having lost the extracted $CO_2$, is diluted to its initial concentration.

• Step 4 → 1: absorbing atmospheric $CO_2$ – diluted solution with depleted DIC concentration is exposed to atmospheric $CO_2$ until a solution partial pressure of $p_{in}$ is reached.

Finally, the main driving mechanism explored in this system is osmotic pressure, resulting in concentrating and diluting the solution, or equivalently adding and removing water (Fig. 1A). This can be done through a number of mechanisms, such as reverse osmosis or capacitive deionization,[28–30] which are not explored in detail here. Our previous study evaluates the work necessary to drive the concentration process.[18,19,27,31] In this work, a lower bound energy analysis is conducted to establish feasibility and evaluate parameter trade-offs.

In general, alkalinity carriers can also be entirely removed if the acid–base system includes some weak base species, however this is not considered in this work. Additionally, the charge state of the acid–base system species can also be used as a basis for separation. For example, nanofiltration membrane separation can be used to separate uncharged and charged species.[32,33]

This work reports the first proof of principle experiment demonstrating the ABCS through a boric acid and polyol experimental system. The system is characterized and its limitations are discussed. A general ABCS theoretical framework is developed to explore requirements for a solution that absorbs $CO_2$ in a diluted state, and then outgasses $CO_2$ when the solution is concentrated. Requirements for the acid–base system are identified to reach adequate acidification as the solution is concentrated. In general, this work builds on the large body of research of non-linear chemical reactions,[24,34] and outlines pathways for theoretical and experimental improvement of the ABCS.

### 2.1 ABCS chemistry: boric acid and polyol

One experimental candidate system exhibiting desired properties is a boric acid and polyol system. Boric acid, $H_3BO_3$, is a very weak acid, with an ionization constant around $pK_a = 9.20$.[26] Boric acid does not react in aqueous solution as a Brønsted acid, but instead, it behaves as a Lewis acid, binding a hydroxide to form the $B(OH)_4^-$ anion:

$$B(OH)_3 + H_2O \xrightleftharpoons{K_a} B(OH)_4^- + H^+ \tag{1}$$
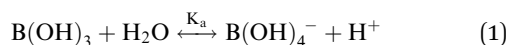
A longstanding experimental observation states that the strength of boric acid can be increased through the addition of organic compounds with at least two hydroxyl groups (polyol), such as mannitol, sorbitol, glycerol, and others. In fact, boric acid reacts with polyols and other polyalcohols, either in a 1 : 1 or 1 : 2 boron to polyol molar ratio, represented by the following two reactions:

$$B(OH)_3 + H_2L \leftrightarrow B(OH)_2L^- + H_2O + H^+ \tag{2}$$

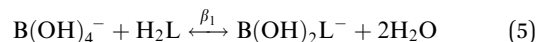$$B(OH)_3 + 2H_2L \leftrightarrow BL_2^- + 3H_2O + H^+ \tag{3}$$
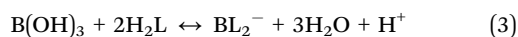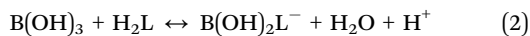
Here, L corresponds to the polyol species. The boric acid disassociation reaction is a first order reaction, while the two reactions above are second and third order reactions, respectively, corresponding to the generalized reaction schemes detailed in the ESI,† in Table C1.

The modified boric acid equilibrium constant, $K_a^*$, replaces $K_a$ in eqn (1) and, as a function of the added polyol, takes the form of ref. 26:

$$K_a^* = K_a \left( 1 + \beta_1[H_2L] + \beta_2[H_2L]^2 \right) \tag{4}$$

Here, $\beta_1$ and $\beta_2$ are experimentally measured equilibrium constants, with $\log(\beta_1) = 3$ and $\log(\beta_2) = 5$,[26] relating to the following reactions (with mannitol as the polyol) where the anion species is treated as the reactant:

$$B(OH)_4^- + H_2L \xrightleftharpoons{\beta_1} B(OH)_2L^- + 2H_2O \tag{5}$$

$$B(OH)_4^- + 2H_2L \xrightleftharpoons{\beta_2} BL_2^- + 4H_2O \tag{6}$$

This reaction scheme can be converted to a system of equations and applied to the ABCS, and all the reactants in this system are commercially-available chemical species that can be studied experimentally. However, the following realizations makes this particular chemical system likely impractical to be realized in a scalable DAC process. First, the DIC system at atmospheric $CO_2$ partial pressure buffers the pH around 9 to 10. And second, the $pK_a$ of boric acid means that much of the acid will be in a disassociated state in this pH range. This negates the cooperative effect from the polyol in the operating regime of the ABCS. In other words, if the post-absorption pH is greater than 9.3 (the boric acid $pK_a$), then a majority of the boric acid is already in the anionic form, and the interaction with polyols will not shift its charge state significantly. To make use of the polyol and boric acid reaction as a driver of the ABCS, the $CO_2$ absorption step would need to bring the pH of the solution below 9, which implies extremely slow absorption kinetics.

Alternatively, cycle output would improve if synthetic chemistry modifications to boric acid complexes were made to increase its $pK_a$, preferably to 10 or higher. Ideally, however, the $pK_a$ of the weak acid is as high as possible, such that deprotonation can occur only through reaction with a complexing agent.

# 3 Materials and methods

## 3.1 Measuring solution states

To characterize the alkalinity, DIC, and boric acid and polyol system, solution states were determined by first measuring the pH of a concentrated solution prepared by mixing dry chemicals in different ratios with diH$_2$O. Then, taking each concentrated solution starting point and measuring the pH of the dilution series, which keeps the chemical ratios constant but reduces the concentration, allows for mapping out the pH-concentration parameter space (Fig. 2A; black dots). An Orion ROSS Micro Electrode was used to measure pH with a Thermo Orion Star A211 Benchtop pH Meter. In this work, alkalinity was introduced as sodium cations. Sodium hydroxide, sodium carbonate, sodium bicarbonate, boric acid, L-sorbitol were all purchased from Sigma-Aldrich.

To map the pH-concentration parameter space, each prepared concentrated solution, at either 0.1 or 1 molal, was measured
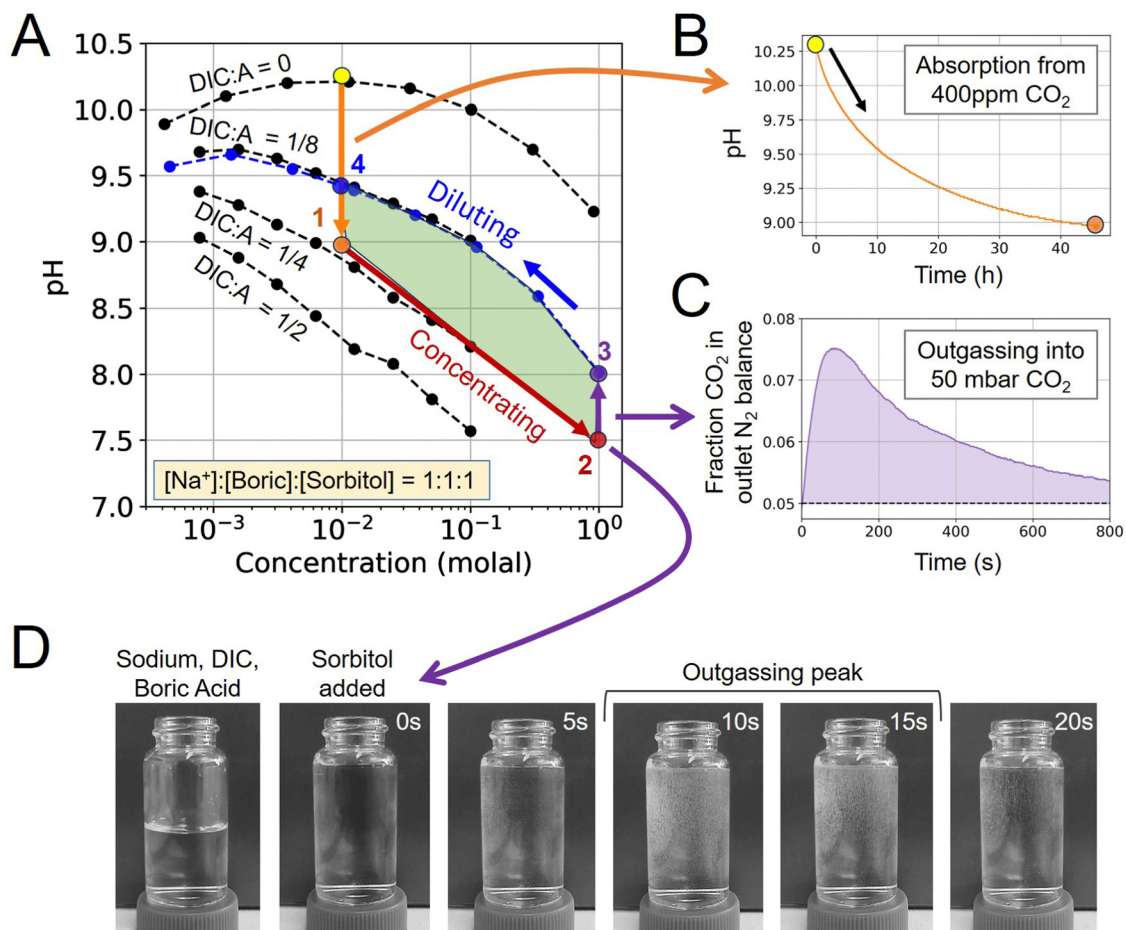
**Fig. 2** Experimental ABCS cycle demonstration. (A) pH-concentration plot, with each point corresponding to an equilibrated solution state locked at a 1 : 1 : 1 sodium : boric-acid : sorbitol concentration. Dashed black lines connect dots at the same DIC-to-alkalinity ratios, with alkalinity being equivalent to $[Na^+]$. (B) Absorption of 10 mM sodium, boric acid, and sorbitol solution with no pre-loaded DIC from 400 ppm $CO_2$ in $N_2$ balance. (C) Direct measurement of $CO_2$ in gaseous phase during outgassing from State 2 into 50 mbar $CO_2$ in $N_2$ balance. (D) Visual confirmation of outgassing. Sorbitol solution was added to a sodium, DIC, and boric acid solution, which triggers $CO_2$ outgassing due to the acidification reaction between sorbitol and boric acid. Image contrast was modified to highlight bubble generation.

immediately after mixing, as well as 30 minutes after mixing to ensure that no significant $CO_2$ outgassing takes place at the given concentration ratio. This ensures that the $CO_2$ partial pressure of the prepared solution is sufficiently close to equilibrium with atmospheric conditions.

Solutions were all prepared with a fixed ratio of sodium, boric acid (B), and sorbitol (S) of: $Na^+ : B : S = 1 : 1 : 1$. Four starting points were chosen with a different DIC-to-alkalinity ratio of 0, 1/8, 1/4, and 1/2. From each starting point, each solution was diluted in series by factors of 1/3 by adding diH$_2$O.

### 3.2 Absorption and outgassing

To study absorption and outgassing rates, a stirred-cell reactor (SCR) setup was assembled (ESI,† Fig. A1). Three mass flow controllers (Sierra SmartTrak 50) were installed in parallel, each connected to its own gas tank: 100% $N_2$, 100% $CO_2$, 0.4 mbar $CO_2$ in $N_2$ balance (gas tanks were purchased from AirGas). Gases were combined and mixed at a known ratio and flow rate, and bubbled through deionized water to moisten the gas feed and reduce

evaporative loss. The gas line was then fed into the SCR, which was installed with conductivity, temperature, and pH probes (ThermoFisher). The SCR was placed on a stir plate and a medium-sized stir bar was spun at 200 rpm. This rpm was chosen so as not to significantly deform the solution surface, but still be fast enough to achieve a well-mixed solution condition and reach the pseudo-first order absorption regime. At 50 mL of solution loading, the gas–liquid surface area was measured to be 0.0029 m$^2$.

For each absorption experiment, 50 mL of solution was loaded into the SCR, and temperature was controlled at 25 C using a water jacket connected to a temperature-controlled water bath. Measurements were continuously recorded onto a computer for analysis. The known solution alkalinity allowed for using pH to calculate $CO_2$ absorption. Gas flow rates were always high enough to deviate in $CO_2$ concentration by <5% due to absorption. Conductivity measurements were used to ensure that evaporative loss was within <5%.

For outgassing experiments, the gas outlet was passed through a 10% infrared $CO_2$ sensor (CO$_2$Meter K30 Sensor) to

measure the change in $CO_2$ partial pressure in nitrogen balance. Outgassing into vacuum was simulated by applying a 50 mbar $CO_2$ in $N_2$ stream to the solution. Outgassing experiments were conducted with 10 mL of solution loaded.

### 3.3 Modeling ideal chemical reactions

To study the relationship between DIC, alkalinity, the weak acid system, and partial pressure, we developed an Aqueous DIC Model (ADICM), which solves the system of equations detailed in Section 4.2.1 and ESI,† Section B. In this theoretical study, we assume dilute solutions in which the activity of any non-solvent species is proportional to its concentration, and therefore chemical relations can be evaluated through concentrations and fixed equilibrium constants. We also assume that there are no solubility constraints in the tested regimes, with final alkalinity conditions being studied up to 3 M. The Python package, SciPy, was used to solve the nonlinear system of equations using the "fsolve" function.

# 4 Results and discussion

### 4.1 Experimental ABCS analysis

To demonstrate the ABCS cycle, the absorption, concentrating, outgassing, and diluting steps were characterized through a combination of 400 ppm $CO_2$ absorption experiments, solution pH measurements, and direct $CO_2$ outgassing measurements into a headspace of 50 mbar of $CO_2$ partial pressure.

First, a solution without any pre-loaded DIC prepared at 10 mM sodium hydroxide, boric acid, and sorbitol, was exposed to 400 ppm $CO_2$ and allowed to reach equilibrium in the absorption module (Step 4 → 1). The pH dropped from 10.27 to 8.98 (Fig. 2B). Using the mapped out pH-concentration space as reference (Fig. 2A; black dots), we infer that the DIC-to-alkalinity ratio increased from 0 to 1/4. This is equivalent to 2.5 mM of DIC loading.

For the concentrating step (Step 1 → 2), a solution was prepared at 1 molal alkalinity concentration, with a 1/4 DIC-to-alkalinity ratio or 0.25 molal DIC, to effectively simulate a concentrating step of 100×. The concentrated solution was loaded into the outgassing module and exposed to 50 mbar $CO_2$ in $N_2$ balance. Outgassed $CO_2$ was measured directly in gas phase to confirm that $CO_2$ can be extracted from this solution condition (Fig. 2C). Initial pH was measured at 7.50 and increased to 8.02 upon equilibration with 50 mbar in the outgassing module (Step 2 → 3).

The post-outgassing solution (State 3) was taken from the outgassing module and the pH of its dilution series was measured (Fig. 2A; blue dots). Based on the pH-concentration parameter space, the DIC-to-alkalinity dropped from 1/4 to 1/8, which means that roughly 0.125 molal of DIC was outgassed. The directly measured gaseous $CO_2$ quantity was found to be within 10% of the solution measurement.

That the four steps enclose a finite area in the pH-concentration space demonstrates the first experimental evidence of the ABCS cycle. The full cycle, at the tested parameters, would

have a volumetric cycle capacity, or $C_{out}$, of 1.25 mM extracted $CO_2$ relative to the feed solution. Under these unoptimized conditions, outgassing into 50 mbar of $CO_2$ occurred on a timescale of minutes, whereas absorption required hours at a measured average absorption flux of 0.40 µmoles m$^{-2}$ s$^{-1}$. In this work, because the chemical conditions are far from optimal for the absorption and cycle capacity, more detailed kinetic analysis was not pursued. However, preliminary findings suggest that absorption promoters are required to make this chemical system competitive with incumbent aqueous DAC technologies.

Finally, a visual inspection of outgassing from the concentrated solution (State 3) was performed in a 25 mL vial (Fig. 2D). Small bubbles were detected within seconds of adding sorbitol to the sodium, boric acid, and DIC solution. We note that outgassing into 50 mbar under flowing headspace exhibits different kinetics than rapid mixing in a vial under ambient conditions.

### 4.2 Generalized ABCS theory

Though the addition of the boric acid and polyol system represents an experimentally feasible ABCS cycle, its cycle capacity and absorption rate are impractical for a scalable DAC process. We therefore develop a theoretical model to identify optimal ABCS chemical properties. This analysis is intended to guide synthetic chemistry work and the search for different applicable chemistry systems.

**4.2.1 Incorporating a weak acid system.** We build on an aqueous DIC model that characterizes the $CO_2$ partial pressure based on alkalinity and DIC concentrations (detailed in ESI,† Section B). We introduce a generalized theoretical weak acid system that allows for evaluating reaction order, concentration, and p$K_a$. This framework allows for mathematically studying arbitrary reaction orders through the following chemical reaction system:

$$(n - 1)L + AH \leftrightarrow L_{n-1}A^- + H^+ \tag{7}$$
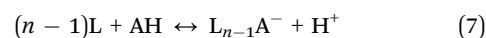
Here, L is a non-charged complexing species that reversibly interacts with the weak acid, AH, to deprotonate it. An nth order reaction means that $n$ reactant species need to react together to form a product and a proton. Therefore, in this scheme, one AH molecule and $n - 1$ L molecules constitute an $n$th order system. We define $K_{a,n}$ as the equilibrium constant for the corresponding $n$th-order reaction. A generalized equilibrium relation can be written in the following way:

$$K_{a,n} = \frac{[L_{n-1}A^-][H^+]}{[L]^{n-1}[AH]} \tag{8}$$

Evaluating the concentration-pH scaling differences helps reveal the strength with which different reaction orders drive the ABCS process. Taking the nth order case as a generalizable example, we study a simplified system where that all protons come from AH (*i.e.* there is no additional proton-based reaction or buffering, and the water dissociation reaction is negligible). This corresponds to a solution without DIC, and implies that

the two products in eqn (7) must be in a 1:1 ratio, so $[L_{n-1}A^-]$ = $[H^+]$.

Because the driver of the ABCS is a concentrating step that increases the concentration of all the non-solvent species together, we define a concentration factor, $\chi$, to characterize the pH-concentration scaling. Mathematically, this is expressed by: $([AH]_2^+ [L_{n-1}A^-]_2 = [AH]_0\chi)$. The subscript "0" represents that the total product and reactant concentration in the pre-concentrated solution (State 1) of the given species, such that: $[AH]_0 = [AH]_1 + [L_{n-1}A^-]_1$. Equivalently, $[AH]_0$ is the initial weak acid concentration dissolved necessary to prepare State 1. The subscripts 1 and 2 correspond to the pre- and post-concentrating condition, respectively. Similarly, the initial complexing agent concentration is defined as follows: $[L]_0 = [L]_1 + [L_{n-1}A^-]_1$. We further simplify the relation by assuming that the acid and complexing species concentrations are at a ratio of $\theta = [L]_0/[AH]_0$. Taking eqn (8) and incorporating the concentration factor perturbation, we derive the following relation:

$$K_{a,n} = \frac{[H^+]^2}{(\theta[AH]_0\chi)^n} \quad (9)$$

Rearranging and taking the log of both sides results in the following scaling relation:

$$pH = -(n/2)\log_{10}(\theta\chi) + \text{const} \quad (10)$$

This relation reveals that the acidification pH increases more sharply with concentration factor at higher reaction orders, suggesting that higher reaction orders are favored in the ABCS. The concentration ratio of complexing agent to weak acid enhances acidification logarithmically. However, we note that this concentration-pH scaling relation will be modified depending on which other acid–base species are added to the solution, and at different molar ratios. A detailed scaling analysis is reported in ESI,† Section C. The concentration-pH scaling for the combined strong base and weak acid system is plotted in Fig. 6: without DIC in panel A and B, and with DIC in panel C and D, revealing the concentration-dependent pH effects that are the basis of the ABCS. ESI,† Table C1 lists the reactions and corresponding equilibrium relations, for a range of conditions, as well as the associated concentration-pH scaling of that particular reaction scheme.

**4.2.2 Optimization analysis.** With a theoretical basis developed, parameter optimization analysis reveals equilibrium relations and initial concentrations that maximize the ABCS cycle capacity, allowing for conditions yielding high $C_{out}$, high output partial pressure and high post-outgassing pH (labeled with a 4 subscript). High $C_{out}$ values reduce water-handling requirements. High output partial pressure increases the outgassing rate and reduces vacuum pumping costs. Higher $pH_4$, which corresponds to higher hydroxide concentration, corresponds to higher absorption rate, which is evident through the dominant absorption reaction pathway: $CO_2 + OH^- \rightarrow HCO_3^-$.[35] Higher absorption rates reduce air–liquid contacting infrastructure costs and required land area. A detailed optimization analysis is conducted in ESI,† Section C.1, finding that higher reaction orders yield more favorable ABCS cycle outputs.

Fig. 3 plots the optimal points for each reaction order, maximizing $C_{out}$ at different strong base ($[B^+]_0$) to weak acid ($[AH]_0$) ratios. Non-intuitive $K_{a,n}$ relations are revealed as
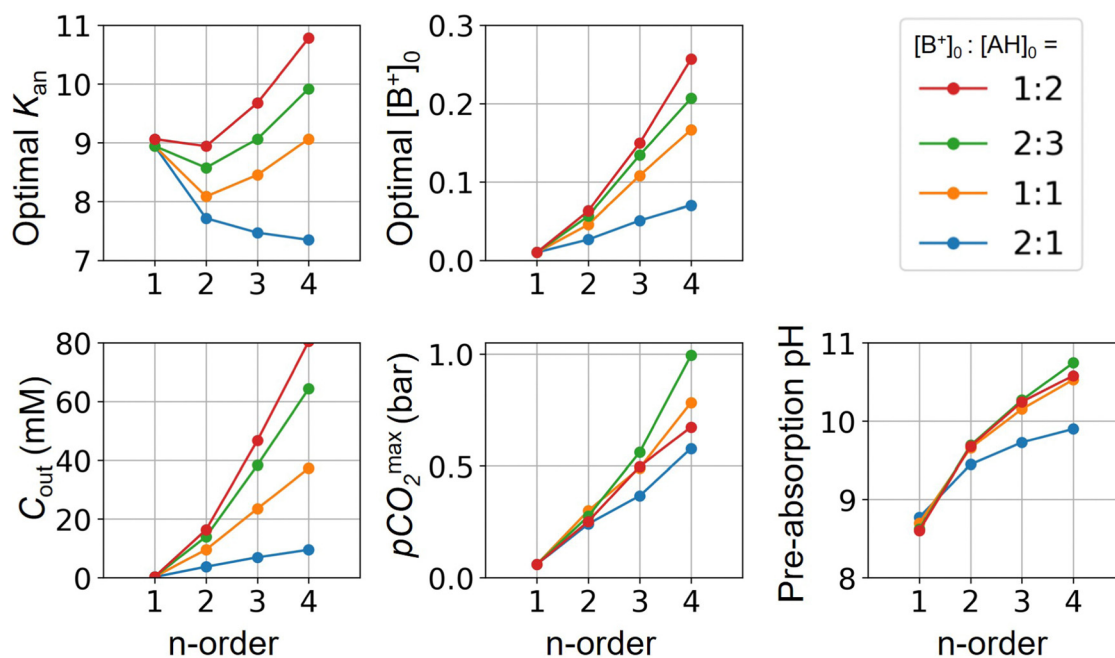


Fig. 3 ABCS optimization analysis. The optimal $n$th-order equilibrium constant ($K_{a,n}$) and initial strong base concentrations ($[B^+]_0$) are reported for each reaction order (1, 2, 3, and 4), and for four strong base (or alkalinity) to weak acid ratios: 2:1, 1:1, 2:3, and 1:2. The corresponding $C_{out}$, $p_{CO_2}^{max}$, and $pH_4$, at each optimal point is plotted. Each optimal point corresponds to the red dot in ESI,† Fig. C2.

**Table 1** Acid–base concentration swing ideal examples. For all conditions: $p_{in}$ = 0.3 mbar; $p_{out}$ = 50 mbar; final alkalinity is set to 2 M. Concentrations and $pK_{a,n}$ values chosen based on optimization results from Fig. 3

| Example | Reaction order | $[B^+]_0 : [AH]_0$ | $[B^+]_0$ (M) | $[AH]_0$ (M) | $[L]_0$ (M) | $pK_{a,n}$ | $C_{out}$ (mM) | $p_{CO_2}^{max}$ (mbar) | $pH_4$ | $E_{CO_2}$ (kJ mol$^{-1}$) |
|---|---|---|---|---|---|---|---|---|---|---|
| 1 | 1st order | 1:1 | 0.01 | 0.01 | 0 | 9.0 | 0.29 | 60 | 8.71 | 1110 |
| 2 | 2nd order | 1:1 | 0.05 | 0.05 | 0.05 | 8.0 | 9.5 | 270 | 9.62 | 165 |
| 3 | 2nd order | 1:2 | 0.05 | 0.1 | 0.1 | 9.0 | 15.6 | 320 | 9.78 | 173 |
| 4 | 2nd order | 1:2 | 0.01 | 0.02 | 0.02 | 9.0 | 5.8 | 1400 | 10.38 | 134 |
| 5 | 3rd order | 1:1 | 0.1 | 0.1 | 0.2 | 8.5 | 23.3 | 540 | 10.21 | 157 |
| 6 | 3rd order | 1:2 | 0.15 | 0.3 | 0.6 | 9.5 | 46.0 | 570 | 10.18 | 165 |
| 7 | 3rd order | 1:2 | 0.01 | 0.02 | 0.04 | 9.5 | 7.1 | 4700 | 11.67 | 145 |

reaction order and base-to-weak-acid ratios are varied. For all conditions, at the optimal point, higher reaction order and higher weak acid to base ratios increase the cycle capacity ($C_{out}$), maximum solution $CO_2$ partial pressure post-concentration but before any extraction $\left(p_{CO_2}^{max}\right)$, and pre-absorption pH ($pH_4$). The output from the optimal $C_{out}$ analysis is used to study ABCS operating conditions in the next section.

Whereas completely optimal conditions are unlikely to be found in existing synthetic or naturally-occurring chemical systems, this analysis serves as a guide for chemical species exploration, as well synthesis targets for chemical design.

**4.2.3 ABCS optimal cycle output.** Given the optimization results from the previous section, we evaluate the ABCS process output as a function of reaction order and starting concentrations. We find a key trade-off such that at lower initial concentrations (alkalinity around 10 mM), higher $CO_2$ partial

pressure and higher post-outgassing pH is reached, whereas the cycle capacity output is lower compared to that from higher initial concentrations (alkalinity around 50 mM or more).

Table 1 reports sample process conditions for different $[B^+]_0$, $[AH]_0$, and $[L]_0$ concentrations, and optimal $pK_{a,n}$ values. For a second order reaction, optimal initial concentration of 50 mM base can reach $C_{out}$ around 15 mM and $pH_4$ of 9.78. Decreasing the initial concentration to 10 mM decreases $C_{out}$ to 5.8 mM, but increases $pH_4$ to 10.38 and more than quadruples the $CO_2$ partial pressure (compare Table 1 Examples 3 and 4).

This trade-off is more substantial for third order reactions. Initial concentrations of 150 mM base outgasses 46 mM, reaches partial pressures above 500 mbar, and post-outgassing pH of 10.18. An initial strong base concentration of 10 mM, however, results in 7 mM of outgassed $CO_2$, but more than 4.5 bar of partial pressure and $pH_4$ of 11.67 (compare Table 1 Examples 6 and 7).
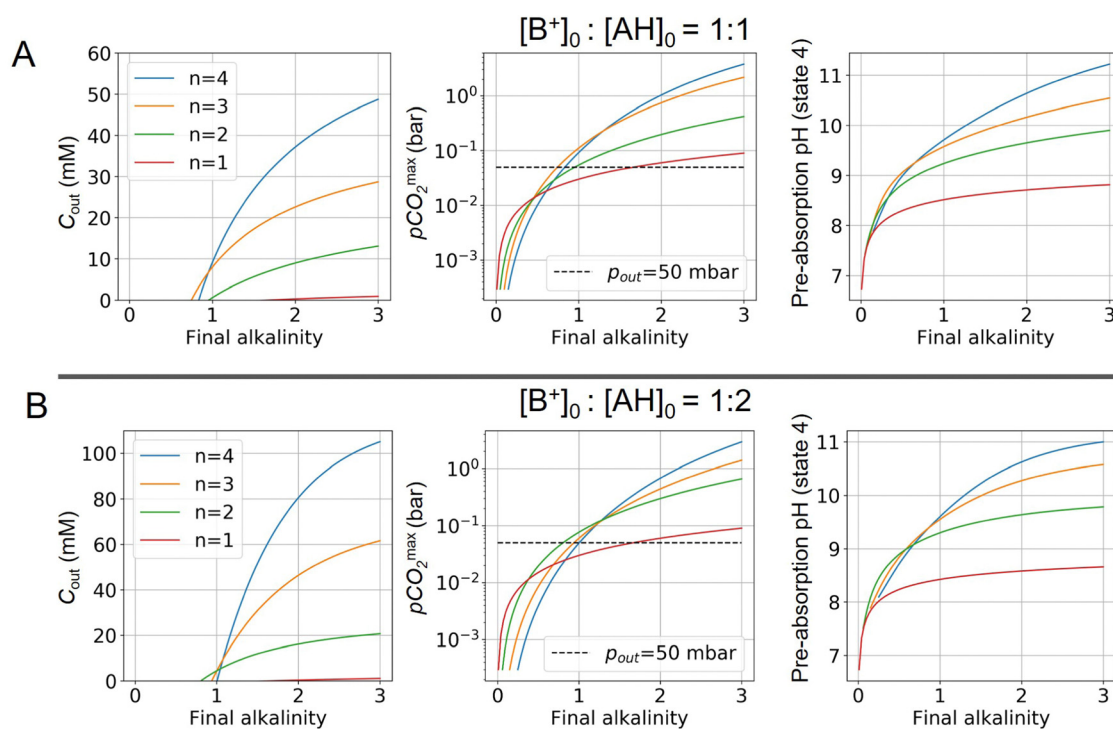


**Fig. 4** ABCS process output. $C_{out}$ (left), $p_{CO_2}^{max}$ (middle), and $pH_4$ (right) are plotted as functions of final alkalinity. (A) $[B^+] : [AH]$ = 1:1; (B) $[B^+] : [AH]$ = 1:2. Each reaction order is modelled with the corresponding optimal initial concentration and $pK_{a,n}$, taken from Fig. 3. For all points, $p_{in}$ = 0.3 mbar; $p_{out}$ is chosen at 50 mbar and denoted with a black dashed line in the middle plots.

Fig. 4 plots $C_{out}$, $p_{CO_2}^{max}$, and $pH_4$, as functions of final alkalinity for a range of reaction orders. Each reaction order is modelled with the corresponding optimal initial strong base concentration and $K_{a,n}$, determined by maximizing $C_{out}$. Parameter map and optimization analysis is reported in ESI,† Fig. S3.

For each reaction order, $C_{out}$ becomes positive at a final alkalinity around 1 M, suggesting that final alkalinity must at least exceed that concentration. Outputs of higher reaction order conditions increase relatively faster as a function of final alkalinity. $C_{out}$ can reach 50 mM for reaction order 4 and 30 mM for reaction order 3, at a 1 : 1 base to weak acid condition (Fig. 4A). When the acid concentration is doubled (Fig. 4B), $C_{out}$ is also roughly doubled for comparable parameter choices.

When optimizing on cycle capacity, the pre-absorption pH falls between 9 and 11 (Fig. 8). Hydroxide-based absorption pathways are still relatively slow for a scalable DAC process in this pH range, suggesting that $CO_2$ absorption promoters, such as carbonic anhydrase, will likely need to be added to the system to reach incumbent technology absorption rates that reach high pH ($>12$) through alkaline solutions.[36,37] It is also possible that certain chemical species that exhibit cooperative acid–base reaction properties will also act as promoters. For example, even boric acid has been shown to have modest $CO_2$ absorption enhancement properties.[38]

**4.2.4 Thermodynamic minimum work for concentrating and outgassing.** To evaluate how the reaction order affects the minimum cycle capture energy, which we define here as the required minimum work for the concentrating and outgassing steps of the ABCS cycle, we apply a thermodynamic minimum model that we derived in previous work:[27]

$$E_{CO_2} = \frac{C_0 RT \ln(\chi)}{C_{out}} + w_{vac}(p_{out}) \quad (11)$$

Here, $C_0$ is the total initial solute concentration in State 1, which includes all the non-solvent species: strong base, weak acid, complexing agent, and DIC. The output is reported in units of kJ per mole of captured $CO_2$. And, $w_{vac}(p_{out})$ is the work necessary to maintain a vacuum at a given outgassing pressure.

Table 1 reports the required minimum energy for seven representative conditions. We find that the thermodynamic minimum energy is approximately 150 kJ mol⁻¹ for reaction orders two and three, for the example parameters and with $p_{in} = 0.3$ mbar, $p_{out} = 50$ mbar, and final alkalinity set to 2 M. The first order reaction, or the base ACS case, requires upwards of 1000 kJ mol⁻¹. This suggests significant benefits when implementing a multi-order system, as compared to a first order chemical reaction. Though the cycle capacity and maximum $CO_2$ partial pressure increase at higher reaction order, there is no significant energy difference across higher reaction orders or specific parameter choices. Based on energy costs of implementing physical reverse osmosis systems, we expect physical energy values to be at least twice the thermodynamic minimum.[39]

For comparison, bench scale redox electrochemical DAC processes have been shown to reach 100 kJ mol⁻¹,[15] and industrial solid sorbent and calcium-looping processes can reach required energy lower than 300 kJ mol⁻¹.[40]

Importantly, whereas the values determined in this section represent an energy minimum, they also do not account for the possibility of energy recovery through the entire thermodynamic cycle. Specifically, during recombination of the concentrated and diluted streams, opportunities for energy recovery exist through forward osmosis or reverse electrodialysis,[41,42] as discussed in previous works evaluating the ACS process.[18,31]

### 4.3 More effective potential acid–base systems

In Section 4.2, we discussed a theoretical framework for a cooperative acid–base system that will outgas $CO_2$ upon concentration, and absorb atmospheric $CO_2$ upon dilution. While the focus of the analysis was on a weak acid and uncharged complexing species, in general, other acid–base schemes can reach the same effective result.

Although we do not explore this theoretical chemical scheme, the cooperative reaction between the weak acid molecules directly, without the need for a complexing agent, would result in a stronger acidification driving force per reactant (for example, $AH + AH \leftrightarrow A_2^{2-} + 2H^+$). In this case, the alkalinity carrier must still be a strong base, such as sodium or potassium.

Alternatively, an intermediate strength base and a weak acid system could achieve desired effects, while reducing the overall concentration of necessary species in solution by eliminating the need for alkalinity carriers, as well as a complexing agent. The following is an example of a second order reaction with such properties: $B^+ + AH \leftrightarrow AB + H^+$. Here, $B^+$ may come from an undissociated molecule, $BOH$, that is strong enough to be disassociated at pH 9–11, but also has affinity to the weak acid.

In general, although different chemical reaction pathways can be envisioned, when searching for desirable candidate chemistry schemes the following chemical and reaction properties should be satisfied: reversible reactions; solubility above 1 M; no DIC interaction; non-volatile; and non-toxic.

## 5 Conclusion

This experimental and theoretical analysis reveals the possibility of the ABCS as a potential approach for direct air capture of $CO_2$. The first-ever proof of principle experiment reported here demonstrates the feasibility of using osmotic pressure and exploiting cooperative acid–base chemistry to drive a DAC cycle. However, the low cycle capacity and slow absorption kinetics in the boric acid and sorbitol system suggest that different non-linear chemical reactants must be explored to find a potentially scalable regime.

Given the guiding principles outlined above, if other reaction schemes can be identified and engineered to have high-order cooperativity then such a process could be competitive with incumbent DAC approaches. Importantly, the ABCS can be driven through reverse osmosis or capacitive deionization modules, which are technologies that are already well

developed and benefit from decades of large-scale deployment. The thermodynamic minimum energy analysis suggests that whereas first-order reaction energies are exceedingly high, second- and third-order ABCS cycles are around 150 kJ mol$^{-1}$. Physical implementations of these systems will likely be a factor of two or more higher, which suggests the need for energy recovery modules, such as forward osmosis, if energy consumption is to be reduced.

It is worth noting, however, that even optimal ABCS cycles still face absorption rate challenges. For third order reaction processes, absorption pH levels can reach above 11, but not above 12, which establishes an upper bound on absorption rate. By comparison, incumbent technologies have engineered their absorption modules around pH closer to 13 or 14.[9] This limitation can be overcome through $CO_2$ absorption promoters.[36,43] Despite this challenge, a significant advantage of the ABCS is its simplicity. The ABCS is driven by a single concentrating step followed by an application of vacuum to extract $CO_2$.

## Data availability

Experimental measurement data for this article is plotted in its entirety in Fig. 2. The code associated with this modeling analysis in this work can be found in Anatoly Rinberg's PhD thesis (2024), Concentrating Alkalinity for Direct Air Capture of Carbon Dioxide: Using Osmotic Pressure for Concentration and Separation, at **https://dash.harvard.edu/handle/1/37377926**.

## Conflicts of interest

There are no conflicts to declare.

## Appendices

### A Absorption and outgassing setup

A setup to measure absorption and outgassing from a candidate solution interacting with a controlled headspace gas was assembled and used for testing absorption from 0.4 mbar of $CO_2$ and outgassing into 50 mbar of $CO_2$ (Fig. 5).

### B Dissolved inorganic carbon equilibrium relations

First, it is worth understanding the pH dependence of the ACS, without any added acid–base species. The charge neutrality condition necessitates:

$$A = b + 2c + K_w/h - h \quad \text{(B1)}$$

Here $A$, $b$, $c$, and $h$ are the alkalinity, bicarbonate, carbonate, and proton concentrations, respectively, and the equilibrium relations between the DIC species are defined as follows:

$$H_{cp} = a/p_{CO_2} \quad \text{(B2)}$$

$$K_1 = \frac{hb}{a} \quad \text{(B3)}$$

$$K_2 = \frac{hc}{b} \quad \text{(B4)}$$

where $a$ corresponds to the aqueous $CO_2$ concentration and $p_{CO_2}$ is the $CO_2$ partial pressure of the gas in equilibrium with the solution. For an accurate treatment, the activity of the species must be considered, however, in this work, we assume dilute solution conditions to simplify the analysis. The conditions for $CO_2$ capture in the ABCS take place roughly with pH between 9 and 11. Therefore, the hydroxide and proton concentrations are much smaller than the rest of the alkalinity and DIC species. Plugging in the DIC equilibrium relations, the above equation can be rewritten as a function of DIC concentration, $C_{DIC}$:

$$A = \frac{h/K_2 + 2}{\dfrac{h^2}{K_1 K_2} + \dfrac{h}{K_2} + 1} C_{DIC} = f_{DIC}(h) C_{DIC} \quad \text{(B5)}$$

Here, $f_{DIC}(h)$ is a function specific to the DIC system that relates alkalinity to $C_{DIC}$ through the proton concentration. This allows for investigating the concentration perturbation, which can be mathematically written through the concentration factor, $\chi$. The concentration factor applies to all non-aqueous species in solution together: $C_i = \chi C_{i,0}$, where $C_i$ is the concentration of species $i$ in solution. Applying the concentration factor perturbation to the DIC system gives:

$$\frac{A}{C_{DIC}} = \frac{\chi A_0}{\chi C_{DIC,0}} = f_{DIC}(h) \quad \text{(B6)}$$
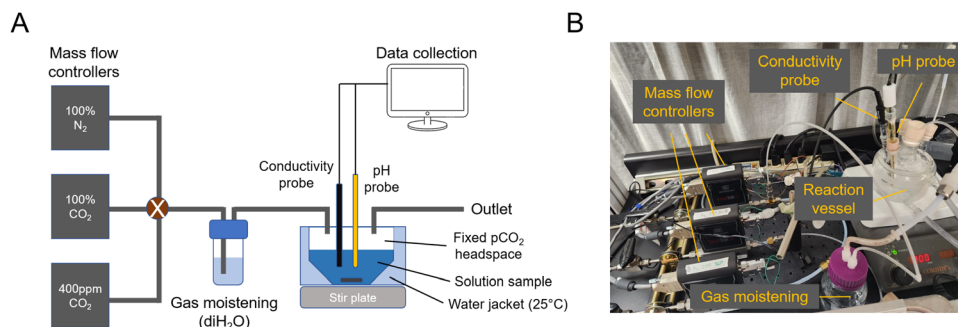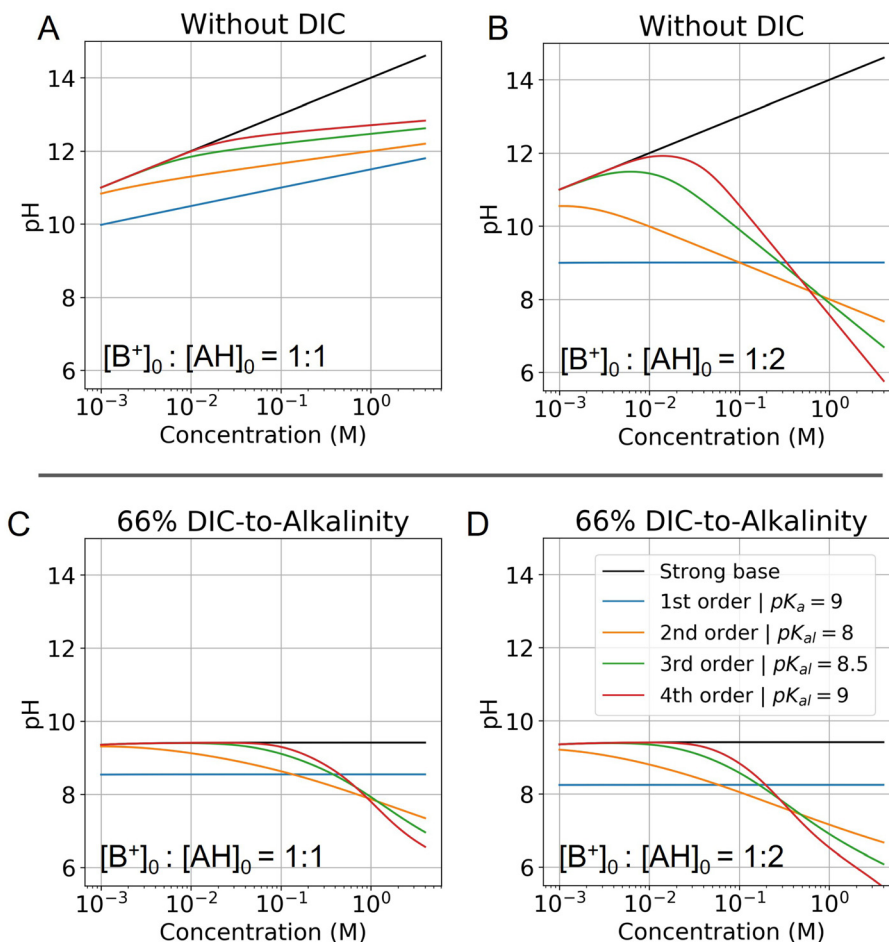


**Fig. 5** Absorption and outgassing setup. (A) Schematic of mass flow controllers and reactor vessel. (B) Image of setup.

**Fig. 6** Modelled pH as a function of fixed concentration. Abscissa corresponds to the concentration of the strong base in solution, and is locked to the weak acid concentration based on the corresponding ratio. (A) pH of a solution with no DIC and a base to weak acid ratio of 1:1 is evaluated for different reaction orders (Table 2). (B) Same conditions, but at a base to weak acid ratio of 1:2 is plotted. (C) Same conditions as (A) are plotted, but with the addition of 66% DIC relative to strong base concentration. (D) Same conditions as (B) are plotted, but with the addition of 66% DIC relative to strong base concentration. Optimal $K_{a,n}$ is picked for each reaction order based on optimization analysis in subsequent sections.

This reveals that, because the $\chi$ terms cancel out, pH is invariant to concentration factor in this regime. In fact, the solution $CO_2$ partial pressure will increase linearly with $\chi$, but will not be further enhanced due to a shift in pH. The black line in Fig. 6C confirms this derivation. In reality, the equilibrium relations, $K_1$ and $K_2$, depend on the ionic strength and will result in a shift in pH as DIC solution is concentrated. Past analyses reveal that the ionic strength increases the outgassing efficiency by a factor of 30–50% depending on the regime,[27] however, these effects are not considered in this work for simplicity.

## C  Weak acid scaling relations

When the ratio of strong base to AH initial concentration is 1:1 (Fig. 6A), the pH increases for all reaction orders, but at varying rates, decreasing with higher reaction order. When the ratio of strong base to AH initial concentration is 1:2 (Fig. 6B), the pH first increases and then decreases as cooperative concentration effects begin to dominate. This non-monotonic effect is present only for reaction orders above 2. It further reveals that is

possible to reach high pH regimes at lower concentrations, and then acidify a solution upon concentrating, which corresponds to the operating principle of ABCS.

Fig. 6C and D plots the concentration pH dependence of a 1:1 and 1:2 strong base to weak acid solution with the DIC system added. This shows that at a given solution loaded with DIC at lower concentration, can be concentrated and acidified, thereby increasing the partial pressure of $CO_2$. Higher weak acid to base ratios increase acidification as a function of concentration, but also lower the concentration point at which the pH deviates from the strong base line. In general, this deviation is due to the fact that at low concentrations AH is entirely associated and uncharged, and so there is no anion to negate the strong base.

Finally, as with the alkalinity and DIC analysis in the previous section, a charge neutrality condition with the weak acid system can be analyzed:

$$[B^+] = [HCO_3^-] + 2[CO_3^{2-}] + [L_{n-1}A^-] + [OH^-] - [H^+] \tag{C1}$$

**Table 2**  Generalized reaction schemes

| Condition | Base | Acid | Reaction | Equilibrium relation | $\chi$ scaling at high conc. |
|---|---|---|---|---|---|
| Strong base | $B^+$ | — | — | — | $\Delta pH \sim \log(\chi)$ |
| 1st order acid | — | AH | $AH \leftrightarrow A^- + H^+$ | $K_{a,1} = \dfrac{[A^-][H^+]}{[AH]}$ | $\Delta pH \sim -(1/2) \times \log(\chi)$ |
| 2nd order acid | — | AH | $L + AH \leftrightarrow LA^- + H^+$ | $K_{a,2} = \dfrac{[LA^-][H^+]}{[L][AH]}$ | $\Delta pH \sim -\log(\chi)$ |
| 3rd order acid | — | AH | $2L + AH \leftrightarrow L_2A^- + H^+$ | $K_{a,3} = \dfrac{[L_2A^-][H^+]}{[L]^2[AH]}$ | $\Delta pH \sim -(3/2) \times \log(\chi)$ |
| nth order acid | — | AH | $(n-1)L + AH \leftrightarrow L_{n-1}A^- + H^+$ | $K_{a,n} = \dfrac{[L_{n-1}A^-][H^+]}{[L]^{n-1}[AH]}$ | $\Delta pH \sim -(n/2) \times \log(\chi)$ |
| Carbonate system | $HCO_3^-$ | $CO_2(aq)$ | $CO_2(aq) + H_2O \leftrightarrow HCO_3^- + H^+$ | $K_1 = \dfrac{[HCO_3^-][H^+]}{[CO_2(aq)]}$ | $\Delta pH \sim -(1/2) \times \log(\chi)$ |
|  | $CO_3^{2-}$ | $HCO_3^-$ | $HCO_3^- \leftrightarrow CO_3^{2-} + H^+$ | $K_2 = \dfrac{[CO_3^{2-}][H^+]}{[HCO_3^-]}$ | $\Delta pH \sim -(1/2) \times \log(\chi)$ |

In the conditions where hydroxide and proton concentrations are significantly smaller than those of the other non-conservative ions, the equation above simplifies to:

$$A = f_{DIC}(h)C_{DIC} + f_{a,n}(h)\alpha^n \qquad (C2)$$

Here, $f_{a,n}(h)$ is a function specific to the nth order condition relating the charge state of the acid to the pH of the solution, and $\alpha$ is the total concentration of the weak acid, assuming that the non-charged species, L, is of equal concentration. Adding the concentration factor perturbation, a pH-$\chi$ dependence is
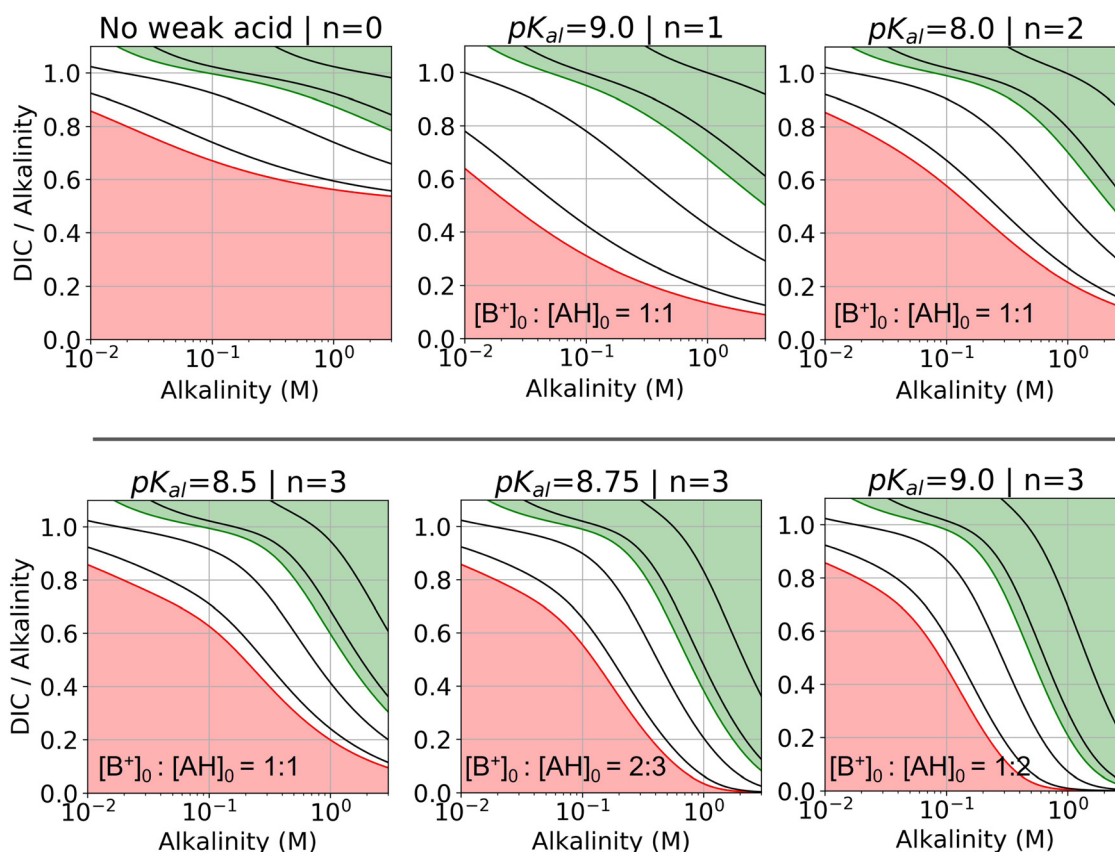


**Fig. 7**  DIC-to-alkalinity diagram for different reaction orders. DIC-to-alkalinity is plotted as a function of initial strong base concentration, or equivalently $[B^+]_0$. The alkalinity to weak acid ratio is specified for each plot. Lines correspond to iso-$pCO_2$ values, with the red line corresponding to 0.4 mbar, and the green line corresponding to 50 mbar. Black lines from bottom up correspond to: 1, 10, 100, and 1000 mbar. Red region is eligible parameter space for absorption, and green region is eligible parameter space for outgassing (given the arbitrary choice of $p_{out}$ = 50 mbar). Optimal $K_{a,n}$ are selected based on optimization analysis in Fig. 3.
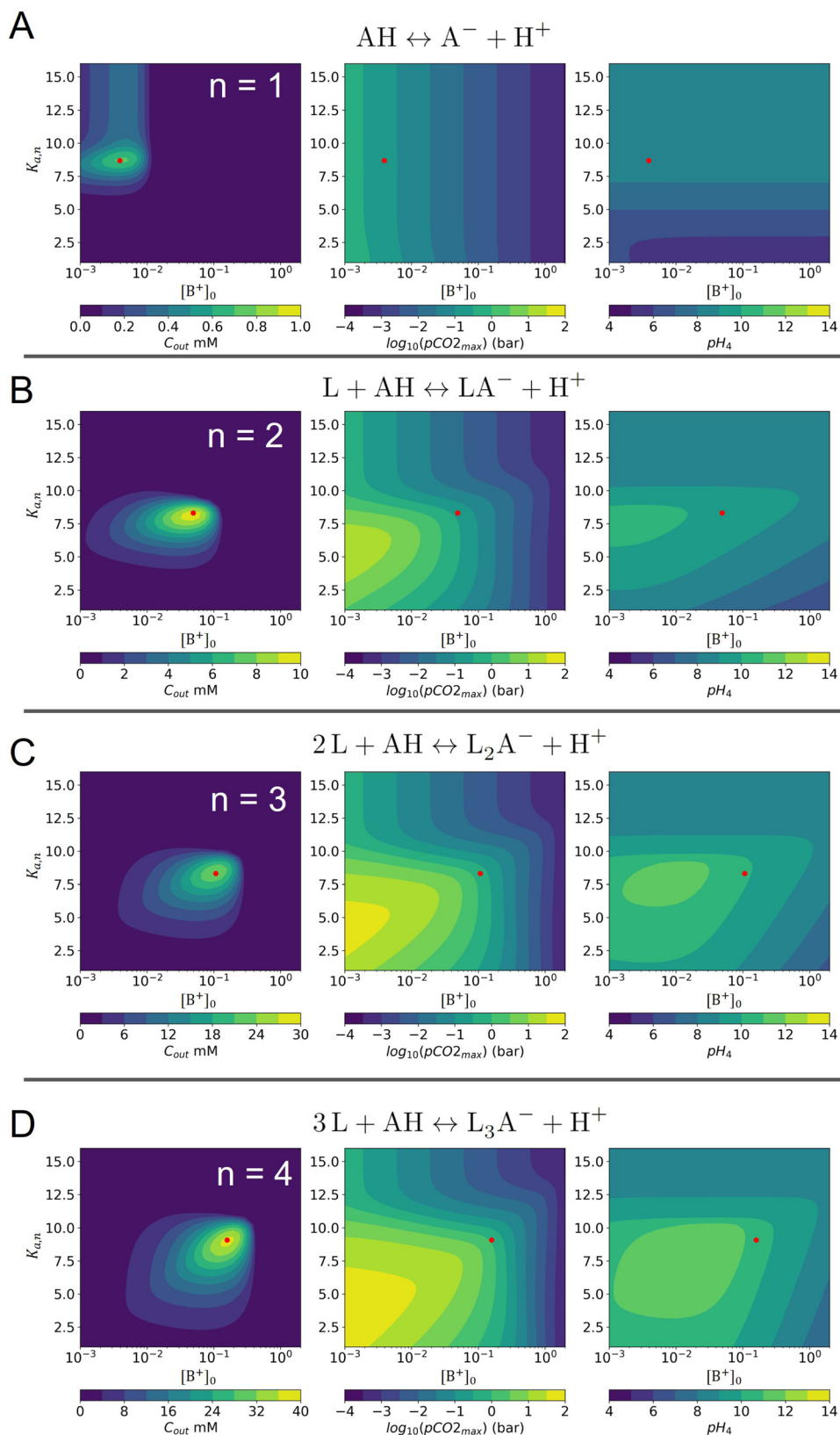
Fig. 8 ABCS output parameter plot. Each point calculates the output from a theoretical ABCS process with corresponding parameters. Contour plots report the $C_{out}$ (left), $p_{CO_2}^{max}$ (middle), and $pH_4$ (right), as a function of $K_{a,n}$ and initial strong base concentration, $[B^+]_0$. For each point, $p_{in} = 0.3$ mbar, $p_{out} = 50$ mbar, and final alkalinity is 2 M. A, B, C, and D correspond to first, second, third, and fourth order reaction conditions; the red dot in each plot corresponds to the optimal $K_{a,n}$ and $[B^+]_0$ value that maximizes $C_{out}$.

revealed:

$$\frac{A_0 - f_{DIC}(h)C_{DIC,0}}{f_{a,n}(h)\alpha_0^n} = \chi^{n-1} \qquad (C3)$$

Inspecting the equations confirms the concentration-dependent pH effects that are the basis of the ABCS. Fig. 6 plots the solution to the equation above for various parameter choices.

**C.1 Parameter space analysis and optimization.** DIC-to-alkalinity diagram analysis in Fig. 7, relating the DIC-to-alkalinity ratio, the alkalinity, $CO_2$ partial pressure, and reaction order, allows for graphically understanding the possible concentration swing improvements at higher reaction orders. Each $x$-axis alkalinity value corresponds to an equivalent strong base concentration, and a fixed ratio of added weak acid (denoted in the bottom of each DIC-to-alkalinity diagram). In other words, at a 1:1 base to weak acid ratio, alkalinity of 0.1 M corresponds to 0.1 M of weak acid. A 1:2 ratio would imply that 0.1 M of alkalinity corresponds to 0.2 M of weak acid. This graphical representation projects to an ideal concentration step when moving right in a fixed DIC-to-alkalinity line, or dilution when moving left.

For all reaction orders, increasing alkalinity concentration results in increasing $CO_2$ partial pressure (Fig. 7). However, higher order reactions compress the iso-$pCO_2$ lines as a function of concentration, which results in a relatively higher partial pressure increase. At higher alkalinity (above 0.1 M), higher reaction orders lowers the DIC-to-alkalinity ratio at 50 mbar (green line), which implies that even more $CO_2$ can be outgassed upon concentration if the same amount of DIC is loaded into solution. Higher weak acid to alkalinity ratios result in further compressing of the iso-$pCO_2$ lines and lowering the DIC-to-alkalinity ratio at 50 mbar (green line) at high concentrations. The $pK_{a,n}$ values for the DIC-to-alkalinity diagrams in Fig. 7 were chosen based on an analysis of optimal $C_{out}$ conditions.

Fig. 8 plots $C_{out}$, $p_{CO_2}^{max}$, and $pH_4$ (pre-absorption pH), as functions of $K_{a,n}$ and initial strong base concentration, $[B^+]_0$. By evaluating this parameter landscape, an optimal $pK_{a,n}$ and $[B^+]_0$ can be chosen to maximize the cycle capacity, $C_{out}$. Plots A, B, C, and D in Fig. 8 correspond to first, second, third, and fourth order reactions at a 1:1 base to weak acid ratio. The red dot corresponds to the optimal parameter point where the process has the largest cycle capacity, revealing the trade-off between maximum $C_{out}$ and absorption rate, which is captured by the $pH_4$ metric. $[B^+]_0$ values that are lower than the optimal red point, can increase the post-outgassing pH by a unit or more, while decreasing the $C_{out}$ value.

## Acknowledgements

## References

1 *Climate Change 2021: The Physical Science Basis. Contribution of Working Group I to the Sixth Assessment Report of the Intergovernmental Panel on Climate Change*, ed. V. Masson-Delmotte, P. Zhai, A. Pirani, S. L. Connors, C. Péan and S. Berger, *et al.*, Cambridge University Press, Cambridge, United Kingdom and New York, NY, USA, 2021.

2 A. Bergman and A. Rinberg, The Case for Carbon Dioxide Removal: From Science to Justice, in *CDR Primer*, 2021. Available from: **https://cdrprimer.org/read/chapter-1**.

3 R. A. Rohde and Z. Hausfather, The Berkeley Earth Land/Ocean Temperature Record, *Earth System Sci. Data*, 2020, **12**(4), 3469–3479. Available from: **https://essd.copernicus.org/articles/12/3469/2020/**.

4 IPCC, Global warming of 1.5 °C, 2018.

5 D. Lenzi, The ethics of negative emissions, *Global Sustainability*, 2018, **1**, e7, DOI: **10.1017/sus.2018.5**.

6 J. C. Minx, W. F. Lamb, M. W. Callaghan, S. Fuss, J. Hilaire and F. Creutzig, *et al.*, Negative emissions—Part 1: Research landscape and synthesis, *Environ. Res. Lett.*, 2018, **13**(6), 063001, DOI: **10.1088/1748-9326/aabf9b**.

7 S. Fuss, W. F. Lamb, M. W. Callaghan, J. Hilaire, F. Creutzig and T. Amann, *et al.*, Negative emissions—Part 2: Costs, potentials and side effects, *Environ. Res. Lett.*, 2018, **13**(6), 063002, DOI: **10.1088/1748-9326/aabf9f**.

8 E. S. Sanz-Pérez, C. R. Murdock, S. A. Didas and C. W. Jones, Direct Capture of $CO_2$ from Ambient Air, *Chem. Rev.*, 2016, **116**(19), 11840–11876, DOI: **10.1021/acs.chemrev.6b00173**.

9 D. W. Keith, G. Holmes, D. St Angelo and K. Heidel, A Process for Capturing $CO_2$ from the Atmosphere, *Joule*, 2018, **2**(8), 1573–1594. Available from: **https://linkinghub.elsevier.com/retrieve/pii/S2542435118302253**.

10 M. Wang, H. J. Herzog and T. A. Hatton, $CO_2$ Capture Using Electrochemically Mediated Amine Regeneration, *Ind. Eng. Chem. Res.*, 2020, **59**(15), 7087–7096, DOI: **10.1021/acs.iecr.9b05307**.

11 Y. Liu, H. Z. Ye, K. M. Diederichsen, T. Van Voorhis and T. A. Hatton, Electrochemically mediated carbon dioxide separation with quinone chemistry in salt-concentrated aqueous media, *Nat. Commun.*, 2020, **11**(1), 2278. Available from: **https://www.nature.com/articles/s41467-020-16150-7**.

12 S. Jin, M. Wu, R. G. Gordon, M. J. Aziz and D. G. Kwabi, pH swing cycle for $CO_2$ capture electrochemically driven through proton-coupled electron transfer, *Energy Environ. Sci.*, 2020, **13**(10), 3706–3722. Available from: **https://pubs.rsc.org/en/content/articlelanding/2020/ee/d0ee01834a**.

13 H. Seo and T. A. Hatton, Electrochemical direct air capture of $CO_2$ using neutral red as reversible redox-active material, *Nat. Commun.*, 2023, **14**(1), 313. Available from: **https://www.nature.com/articles/s41467-023-35866-w**.

14 A. Sodiq, Y. Abdullatif, B. Aissa, A. Ostovar, N. Nassar and M. El-Naas, *et al.*, A review on progress made in direct air capture of $CO_2$, *Environ. Technol. Innovation*, 2023, **29**, 102991. Available from: **https://www.sciencedirect.com/science/article/pii/S235218642200414X**.

15 T. N. D. Cao, S. W. Snyder, Y. I. Lin, Y. J. Lin, S. Negi and S. Y. Pan, Unraveling the Potential of Electrochemical pH-Swing Processes for Carbon Dioxide Capture and Utilization, *Ind. Eng. Chem. Res.*, 2023, **62**(49), 20979–20995, DOI: **10.1021/acs.iecr.3c02183**.

16 G. Liu, A. Yang and R. C. Darton, Numerical Modeling and Comparative Analysis of Electrolysis and Electrodialysis Systems for Direct Air Capture, *ACS Sustainable Chem. Eng.*, 2024, **12**(10), 3951–3965, DOI: **10.1021/acssuscheng.3c06259**.

17 A. Rinberg and M. J. Aziz, Bicarbonate-Carbonate Selectivity through Nanofiltration for Direct Air Capture of Carbon Dioxide, *ACS ES&T Eng.*, 2024, **4**(8), 1959–1969, DOI: **10.1021/acsestengg.4c00150**.

18 A. Rinberg, Concentrating Alkalinity for Direct Air Capture of Carbon Dioxide: Using Osmotic Pressure for Concentration and Separation, 2024, Available from: **https://dash.harvard.edu/handle/1/37377926**.

19 A. M. Bergman, Using Capacitive Deionization for Direct Air Capture of Carbon Dioxide: Theory and Demonstration of the Bicarbonate-Enriched Alkalinity Concentration Swing, 2024, Available from: **https://dash.harvard.edu/handle/1/37377928**.

20 I. R. Epstein and K. Showalter, Nonlinear Chemical Dynamics: Oscillations, Patterns, and Chaos, *J. Phys. Chem.*, 1996, **100**(31), 13132–13147, DOI: **10.1021/jp953547m**.

21 F. Sagués and I. R. Epstein, Nonlinear chemical dynamics, *Dalton Trans.*, 2003, (7), 1201–1217. Available from: **https://pubs.rsc.org/en/content/articlelanding/2003/dt/b210932h**.

22 M. Orbán, K. Kurin-Csörgei and I. R. Epstein, pH-regulated chemical oscillators, *Acc. Chem. Res.*, 2015, **48**(3), 593–601.

23 E. Poros, V. Horváth, K. Kurin-Csörgei, I. R. Epstein and M. Orbán, Generation of pH-Oscillations in Closed Chemical Systems: Method and Applications, *J. Am. Chem. Soc.*, 2011, **133**(18), 7174–7179, DOI: **10.1021/ja2010835**.

24 K. Kovacs, R. E. McIlwaine, S. K. Scott and A. F. Taylor, pH oscillations and bistability in the methylene glycol–sulfite–gluconolactone reaction, *Phys. Chem. Chem. Phys.*, 2007, **9**(28), 3711–3716. Available from: **https://pubs.rsc.org/en/content/articlelanding/2007/cp/b704407k**.

25 Controlling chaos in the Belousov—Zhabotinsky reaction | Nature. Available from: **https://www.nature.com/articles/361240a0**.

26 M. C. C. Azevedo and A. M. V. Cavaleiro, The Acid–Base Titration of a Very Weak Acid: Boric Acid, *J. Chem. Educ.*, 2012, **89**(6), 767–770, DOI: **10.1021/ed200180j**.

27 A. Rinberg, A. M. Bergman, D. P. Schrag and M. J. Aziz, Alkalinity Concentration Swing for Direct Air Capture of Carbon Dioxide, *ChemSusChem*, 2021, **14**(20), 4439–4453. eprint: **https://onlinelibrary.wiley.com/doi/pdf/10.1002/cssc.202100786**.

28 Ion Selectivity in Brackish Water Desalination by Reverse Osmosis: Theory, Measurements, and Implications, *Environ. Sci. Technol. Lett.*, 2020, **7**(1), 42–47, DOI: **10.1021/acs.estlett.9b00686**.

29 Y. S. Oren and P. M. Biesheuvel, Theory of Ion and Water Transport in Reverse-Osmosis Membranes, *Phys. Rev. Appl.*, 2018, **9**(2), 024034, DOI: **10.1103/PhysRevApplied.9.024034**.

30 M. E. Suss, S. Porada, X. Sun, P. M. Biesheuvel, J. Yoon and V. Presser, Water desalination via capacitive deionization: what is it and what can we expect from it?, *Energy Environ. Sci.*, 2015, **8**(8), 2296–2319. Available from: **https://pubs.rsc.org/en/content/articlelanding/2015/ee/c5ee00519a**.

31 A. Rinberg, A. M. Bergman, M. J. Aziz and D. P. Schrag, *Experimental Demonstration of Alkalinity Concentration Swing for Direct Air Capture of $CO_2$*. Harvard Univ., Cambridge, MA (United States), 2023. Available from: **https://www.osti.gov/biblio/2248073**.

32 R. He, C. Dong, S. Xu, C. Liu, S. Zhao and T. He, Unprecedented $Mg^{2+}/Li^+$ separation using layer-by-layer based nanofiltration hollow fiber membranes, *Desalination*, 2022, **525**, 115492. Available from: **https://www.sciencedirect.com/science/article/pii/S0011916421005634**.

33 B. Van der Bruggen, A. Koninckx and C. Vandecasteele, Separation of monovalent and divalent ions from aqueous solution by electrodialysis and nanofiltration, *Water Res.*, 2004, **38**(5), 1347–1353. Available from: **https://www.sciencedirect.com/science/article/pii/S0043135403006420**.

34 T. K. Gustafsson and K. V. Waller, Nonlinear and adaptive control of pH, *Ind. Eng. Chem. Res.*, 1992, **31**(12), 2681–2693. Available from: **https://pubs.acs.org/doi/pdf/10.1021/ie00012a009**.

35 X. Wang, W. Conway, R. Burns, N. McCann and M. Maeder, Comprehensive Study of the Hydration and Dehydration Reactions of Carbon Dioxide in Aqueous Solution, *J. Phys. Chem. A*, 2010, **114**(4), 1734–1740, Available from: **https://pubs.acs.org/doi/pdf/10.1021/jp909019u**.

36 S. S. W. Effendi and I. S. Ng, The prospective and potential of carbonic anhydrase for carbon dioxide sequestration: a critical review, *Process Biochem.*, 2019, **87**, 55–65. Available from: **https://www.sciencedirect.com/science/article/pii/S1359511319310037**.

37 A. de Oliveira Maciel, P. Christakopoulos, U. Rova and I. Antonopoulou, Carbonic anhydrase to boost $CO_2$ sequestration: Improving carbon capture utilization and storage (CCUS), *Chemosphere*, 2022, **299**, 134419. Available from: **https://www.sciencedirect.com/science/article/pii/S0045653522009122**.

38 U. K. Ghosh, S. E. Kentish and G. W. Stevens, Absorption of carbon dioxide into aqueous potassium carbonate promoted by boric acid, *Energy Proc.*, 2009, **1**(1), 1075–1081. Available from: **https://www.sciencedirect.com/science/article/pii/S187661020900143X**.

39 M. Elimelech and W. A. Phillip, The Future of Seawater Desalination: Energy, Technology, and the Environment, *Science*, 2011, **333**(6043), 712–717. Available from: **https://science.sciencemag.org/content/333/6043/712**.

40 S. Pacala, M. Al-Kaisi, M. Barteau, E. Belmont, S. Benson and R. Birdsey, *et al.*, *Negative Emissions Technologies and Reliable Sequestration: A Research Agenda*, The National Academies Press, Washington, DC, 2019, DOI: **10.17226/25259**.

41 Effect of Different Draw Solutions on Concentration Polarization in a Forward Osmosis Process: Theoretical Modeling and Experimental Validation. Industrial & Engineering Chemistry Research, Available from: **https://pubs.acs.org/doi/full/10.1021/acs.iecr.2c03723**.

42 R. A. Tufa, S. Pawlowski, J. Veerman, K. Bouzek, E. Fontananova and G. di Profio, *et al.*, Progress and prospects in reverse electrodialysis for salinity gradient energy conversion and storage, *Appl. Energy*, 2018, **225**, 290–331. Available from: **https://www.sciencedirect.com/science/article/pii/S0306261918306792**.

43 P. C. Tseng, W. S. Ho and D. W. Savage, Carbon dioxide absorption into promoted carbonate solutions, *AIChE J.*, 1988, **34**(6), 922–931. eprint: **https://onlinelibrary.wiley.com/doi/pdf/10.1002/aic.690340604**.